CHEMISTRY
A European Journal

Supporting Information

# Molecular Engineering of $Mn^{II}$ Diamine Diketonate Precursors for the Vapor Deposition of Manganese Oxide Nanostructures

Chiara Maccato,[a] Lorenzo Bigiani,[a] Giorgio Carraro,[a] Alberto Gasparotto,[a] Roberta Seraglia,[b] Jiyeon Kim,[c] Anjana Devi,[c] Gloria Tabacchi,*[d] Ettore Fois,[d] Giuseppe Pace,[b] Vito Di Noto,[e] and Davide Barreca*[b]

chem_201703423_sm_miscellaneous_information.pdf

## Author Contributions

C.M. Conceptualization: Lead; Data curation: Equal; Funding acquisition: Lead; Writing – original draft: Lead
G.T. Conceptualization: Lead; Methodology: Lead; Project administration: Lead; Supervision: Lead
D.B. Conceptualization: Lead; Investigation: Lead; Validation: Lead; Writing – review & editing: Lead.

## 1. Structural characterization

**Table S1.** Crystallographic data and refinement details for $Mn(hfa)_2$•TMEDA and $Mn(tfa)_2$•TMEDA.

| **Compound** | **$Mn(hfa)_2$•TMEDA** | **$Mn(tfa)_2$•TMEDA** |
|---|---|---|
| Chemical formula | $C_{16}H_{18}O_4N_2F_{12}Mn$ | $C_{16}H_{24}O_4N_2F_6Mn$ |
| Formula weight ($g \times mol^{-1}$) | 585.26 | 477.31 |
| Temperature (K) | 114.9(2) | 115.55(10) |
| λ (Å) | 1.54184 | 1.54184 |
| Crystal system | monoclinic | monoclinic |
| Space group | $P2_1/n$ | $P2_1/c$ |
| *a* (Å) | 10.66200(13) | 7.95800(17) |
| *b* (Å) | 14.98128(18) | 20.5098(4) |
| *c* (Å) | 14.9273(2) | 12.9134(3) |
| *β* (°) | 102.7752(13) | 90.536(2) |
| Volume ($Å^3$) | 2325.32(5) | 2107.58(7) |
| *Z* | 4 | 4 |
| $D_{calc}$ ($g \times cm^{-3}$) | 1.672 | 1.504 |
| Absorption coefficient ($mm^{-1}$) | 5.778 | 5.808 |
| *F*(000) | 1172.0 | 980.0 |
| 2*θ* range for data collection (°) | 8.470– 152.432 | 8.092 – 152.184 |
| Reflections collected/unique | 23682/4824 [$R_{int}$ = 0.0395] | 11992/4111 [$R_{int}$ = 0.0280] |
| Data/restraints/parameters | 4824/99/320 | 4111/0/268 |
| Final R indices [$I > 2\sigma(I)$] | $R_1$ = 0.0364, w$R_2$ = 0.0940 | $R_1$ = 0.0360, w$R_2$ = 0.0921 |
| *R* indices (all data) | $R_1$ = 0.0385, w$R_2$ = 0.0957 | $R_1$ = 0.0403, w$R_2$ = 0.0948 |
| goodness-of-fit on $F^2$ | 1.032 | 1.071 |

**Table S2.** Geometrical data calculated for $Mn(hfa)_2$•TMEDA and $Mn(tfa)_2$•TMEDA in the sextet spin state.[a]

| | **$Mn(hfa)_2$•TMEDA** | **$Mn(tfa)_2$•TMEDA** |
|---|---|---|
| **Bond lengths (Å)** | | |
| **Mn–O(1)** | 2.123 | 2.117 |
| **Mn–O(2)** | 2.128 | 2.120 |
| **Mn–O(3)** | 2.128 | 2.120 |
| **Mn–O(4)** | 2.123 | 2.117 |
| **Mn–N(1)** | 2.248 | 2.303 |
| **Mn–N(2)** | 2.248 | 2.303 |
| **O(1)–C(7)** | 1.244 | 1.250 |
| **O(2)–C(9)** | 1.241 | 1.244 |
| **O(3)–C(12)** | 1.241 | 1.244 |
| **O(4)–C(14)** | 1.244 | 1.250 |
| | | |
| **Bond angles (°)** | | |
| **O(1)−Mn−O(2)** | 81.9 | 82.7 |
| **O(3)−Mn−O(4)** | 81.9 | 82.7 |
| **N(1)−Mn−N(2)** | 81.4 | 79.5 |
| **O(1)–Mn–O(4)** | 171.5 | 177.3 |
| **O(3)–Mn–N(1)** | 171.6 | 165.3 |
| **O(2)–Mn–N(2)** | 171.6 | 165.3 |
| **Mn−O(1)−C(7)** | 124.7 | 128.3 |
| **Mn−O(2)−C(9)** | 123.7 | 132.1 |
| **Mn−O(3)−C(12)** | 123.7 | 132.1 |
| **Mn−O(4)−C(14)** | 124.7 | 128.3 |

[a]As the calculated energy differences between the sextet and the doublet spin states amounted to 41.9 kcal×mol$^{-1}$ [$Mn(hfa)_2$•TMEDA] and 44.1 kcal×mol$^{-1}$ [$Mn(tfa)_2$•TMEDA] in favour of the sextet, and those between sextet and quartet were 35.6 kcal×mol$^{-1}$ [$Mn(hfa)_2$•TMEDA] and 39.7 kcal×mol$^{-1}$ [$Mn(tfa)_2$•TMEDA], the spin state of the two complexes was unambiguously defined as a sextet.

## 2. Electronic structure analysis

**Table S3.** NBO charges calculated for atoms in the Mn coordination sphere and the TMEDA, L=hfa/tfa ligands in **Mn(hfa)$_2$•TMEDA (1)** and **Mn(tfa)$_2$•TMEDA (2)**. Atom labels as in Figure 1.

| | **Total Charge** | | ***α* spin** | | ***β* spin** | |
|---|---|---|---|---|---|---|
| | **(1)** | **(2)** | **(1)** | **(2)** | **(1)** | **(2)** |
| Mn | 0.981 | 1.037 | −1.835 | −1.798 | 2.816 | 2.835 |
| N(1) | −0.590 | −0.583 | −0.308 | −0.307 | −0.282 | −0.276 |
| N(2) | −0.590 | −0.583 | −0.308 | −0.307 | −0.282 | −0.276 |
| O(1) | −0.692 | −0.721 | −0.357 | −0.374 | −0.334 | −0.347 |
| O(2) | −0.676 | −0.696 | −0.348 | −0.362 | −0.327 | −0.334 |
| O(3) | −0.676 | −0.696 | −0.348 | −0.362 | −0.327 | −0.334 |
| O(4) | −0.692 | −0.721 | −0.357 | −0.374 | −0.334 | −0.347 |
| L | −0.635 | −0.639 | −0.376 | −0.371 | −0.265 | −0.233 |
| TMEDA | 0.290 | 0.241 | 0.077 | 0.050 | 0.213 | 0.191 |

**Comment to Table S3.** The Natural Bond Orbital (NBO)[1] charge analysis indicates that a significant portion of electronic charge (*i.e.* 1.02 *e* and 0.96 *e* in Mn(hfa)$_2$•TMEDA and Mn(tfa)$_2$•TMEDA complexes, respectively) has been donated by the ligands to the metal center. Nevertheless, the six atoms bonded to Mn still bear a significant fraction of negative charge, indicating that electron density donation also occurs from ligand atoms far away from the metal center. Overall, whereas each hfa donates to Mn 0.365 *e* and 0.361 *e* in Mn(hfa)$_2$•TMEDA and Mn(tfa)$_2$•TMEDA, respectively, the corresponding charge fractions transferred by TMEDA are 0.290 *e* and 0.241 *e*, respectively. Hence, in both cases, and particularly for Mn(tfa)$_2$•TMEDA, the diketonate is a stronger electron donor compared to the diamine. Also, the total electronic charge donated by TMEDA depends on the nature of the diketonate ligand, and is higher for Mn(hfa)$_2$•TMEDA.

**Table S4.** Bond orders calculated for $Mn(hfa)_2$•TMEDA and $Mn(tfa)_2$•TMEDA.[1]

| **bond** | $Mn(hfa)_2$•TMEDA | $Mn(tfa)_2$•TMEDA |
|---|---|---|
| Mn-N(1) | 0.180 | 0.167 |
| Mn-N(2) | 0.180 | 0.167 |
| Mn-O(1) | 0.323 | 0.318 |
| Mn-O(2) | 0.309 | 0.314 |
| Mn-O(3) | 0.309 | 0.314 |
| Mn-O(4) | 0.323 | 0.318 |

**Comment to Table S4**. The reported bond orders[1]are an estimate of the relative strengths of the Mn–N and Mn–O interactions in the two investigated complexes. Compared with the average Mn–O bond orders, the corresponding Mn–N values are by 57% and 53% lower for $Mn(hfa)_2$•TMEDA and $Mn(tfa)_2$•TMEDA, respectively, indicating that the Mn–N bonds are significantly weaker than the Mn–O ones.

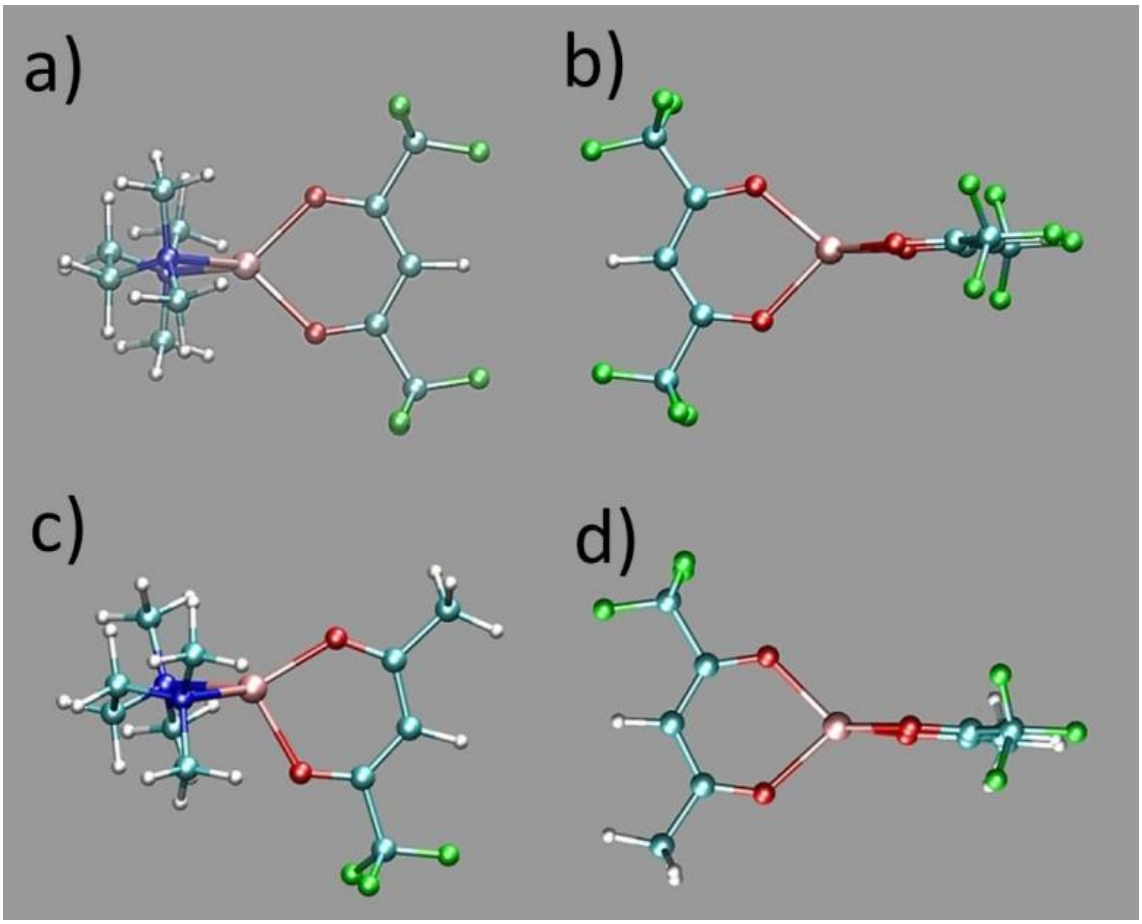


**Figure S1.** Graphical representation of the calculated optimized structure of Mn-containing fragments: (a) Mn(hfa)•TMEDA$^{+}$, obtained by the loss of a hfa ligand from Mn(hfa)$_2$•TMEDA; (b) Mn(hfa)$_2$, obtained by the loss of the TMEDA ligand from Mn(hfa)$_2$•TMEDA; (c) Mn(tfa)•TMEDA$^{+}$, obtained by loss of a tfa ligand from Mn(tfa)$_2$•TMEDA; (d) Mn(tfa)$_2$, obtained by the loss of the TMEDA ligand from Mn(tfa)$_2$•TMEDA. All the fragments are in the sextet spin state. The stabilization energies of the sextet with respect to the quartet were 27.0 kcal×mol$^{-1}$, 26.8 kcal×mol$^{-1}$, 36.5 kcal×mol$^{-1}$ and 35.2 kcal×mol$^{-1}$ for Mn(hfa)•TMEDA$^{+}$, Mn(tfa)•TMEDA$^{+}$, Mn(hfa)$_2$, and Mn(tfa)$_2$, respectively. Atom color codes: Mn=pink; F=green; O=red; N=blue; C=cyano; H=white.

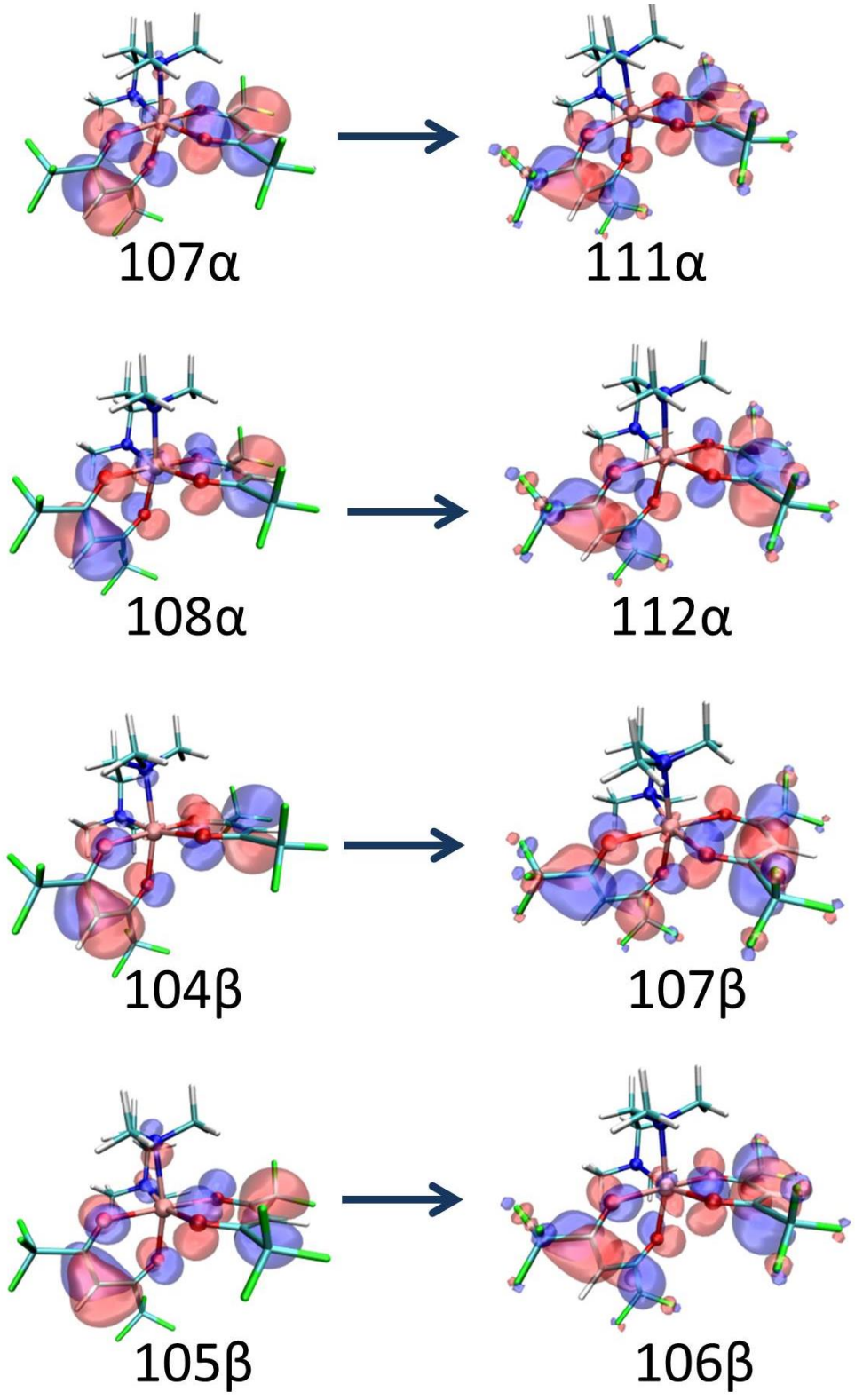


**Figure S2.** The four components of π–π* ligand-to-ligand electronic transitions calculated for $Mn(hfa)_2$•TMEDA at λ = 265 nm and 269 nm (oscillator strength = 0.178 and 0.371), in vacuum and ethanol (the solvent used for the experimental spectrum) respectively, corresponding to the band at λ = 307 nm in the experimental UV-Vis spectrum. The singly occupied molecular orbitals (SOMOs) involved in each component are also shown. Blue and red colors mark positive and negative phases, respectively. Atom color codes as in Figure S1.

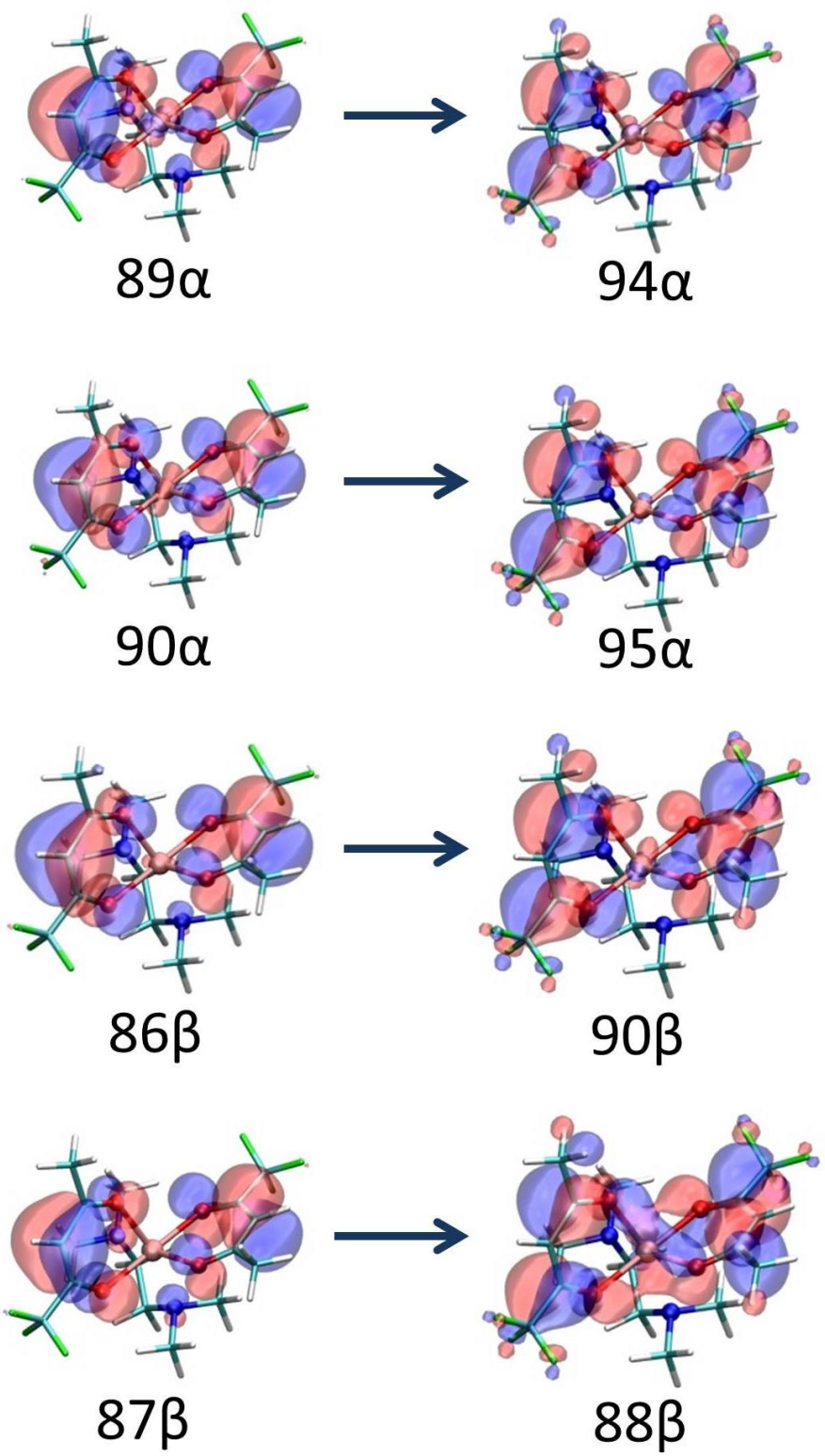


**Figure S3.** The four components of π–π* ligand-to-ligand electronic transitions calculated for $Mn(tfa)_2$•TMEDA at λ = 255 nm and 260 nm (oscillator strength=0.408 and 0.289), in vacuum and ethanol, respectively, corresponding to the band at λ = 296 nm in the experimental UV-vis spectrum. The SOMOs involved in each component are also shown. Blue and red colors mark positive and negative phases, respectively. Atom color codes as in Figure S1.

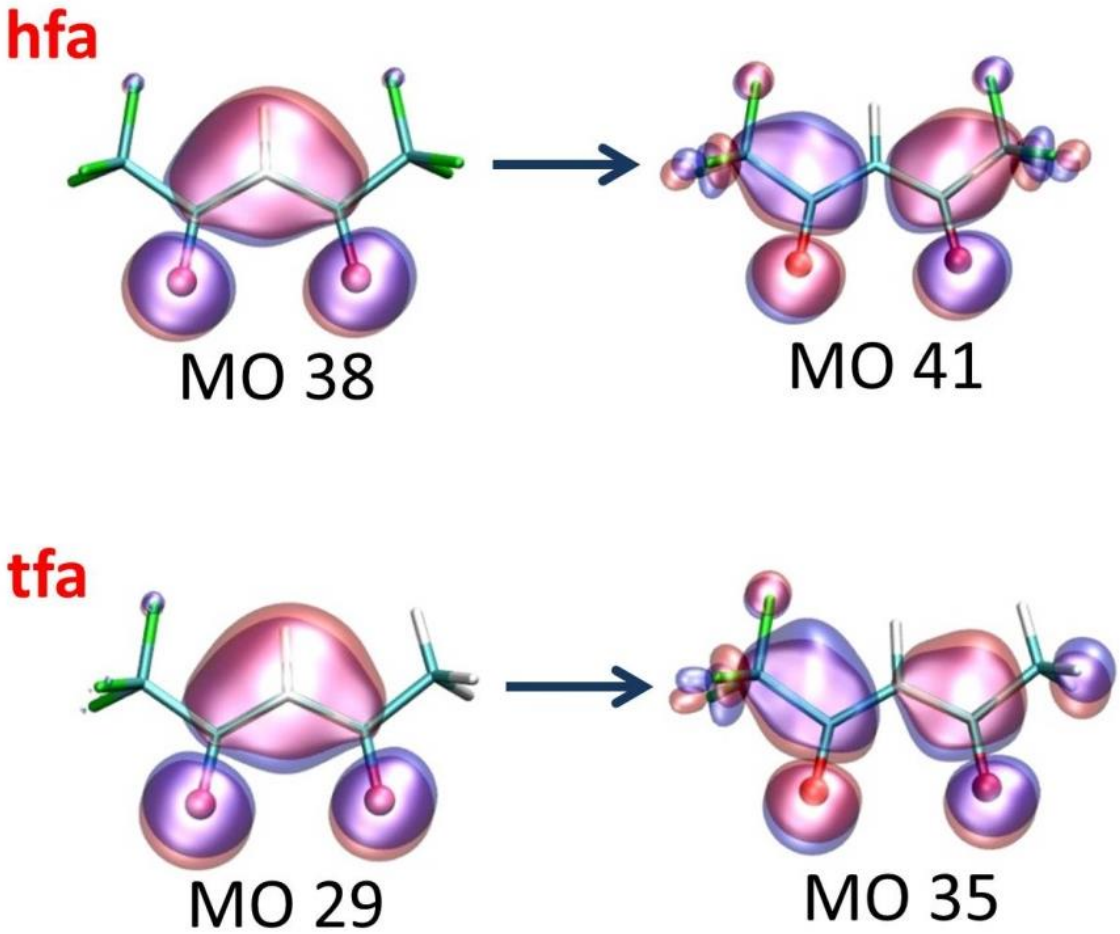


**Figure S4.** Molecular orbitals (MO) involved in the π–π* electronic transitions calculated for the isolated hfa (top) and tfa (bottom) ligands. Both excitations are found in the UV range, at λ = 252 nm for hfa (oscillator strength=0.408) and at 247 nm for tfa (oscillator strength=0.437). Blue and red colors mark positive and negative phases, respectively. Atom color codes as in Figure S1.

**Table S5.** Mn–O and Mn–N distances (Å), stabilization energies (kcal×mol$^{-1}$), and dipole moments (D) calculated for Mn(hfa)$_2$•TMEDA and Mn(tfa)$_2$•TMEDA in a uniform external electric field of magnitude 0.002 a.u. (1.028×10$^8$ V×m$^{-1}$). The corresponding values calculated in the absence of electric field are included for comparison.

| | **Mn(hfa)$_2$•TMEDA** | | **Mn(tfa)$_2$•TMEDA** | |
|---|---|---|---|---|
| | **No field** | **With electric field** | **No field** | **With electric field** |
| Mn–O(1) | 2.123 | 2.124 | 2.117 | 2.117 |
| Mn–O(2) | 2.128 | 2.129 | 2.120 | 2.120 |
| Mn–O(3) | 2.128 | 2.129 | 2.120 | 2.120 |
| Mn–O(4) | 2.123 | 2.124 | 2.117 | 2.117 |
| Mn–N(1) | 2.248 | 2.247 | 2.303 | 2.302 |
| Mn–N(2) | 2.248 | 2.247 | 2.303 | 2.302 |
| ΔE | - | 0.39 | - | 0.07 |
| μ | 7.88 | 8.09 | 1.31 | 1.51 |

**Comment to Table S5.** The electric field strength used for the calculations, larger than those typically employed in ESI-MS experiment (10$^6$÷10$^7$ V×m$^{-1}$), has been chosen in order to emphasize the resulting effects on the structural and electric response properties of the investigated complexes. Nonetheless, the comparison between values obtained with and without external field indicates that structural changes, electronic structure perturbation, and energetic stabilization induced by the field itself are very small. It may be therefore deduced that external electric fields of such magnitudes should have significant effects only on the complex orientation, corresponding to the alignment of the molecular dipole with the external field. Such effects would closely depend on the magnitude of the electric dipole moment of ML$_2$•TMEDA (L=hfa/tfa).

## 3. ESI-MS characterization

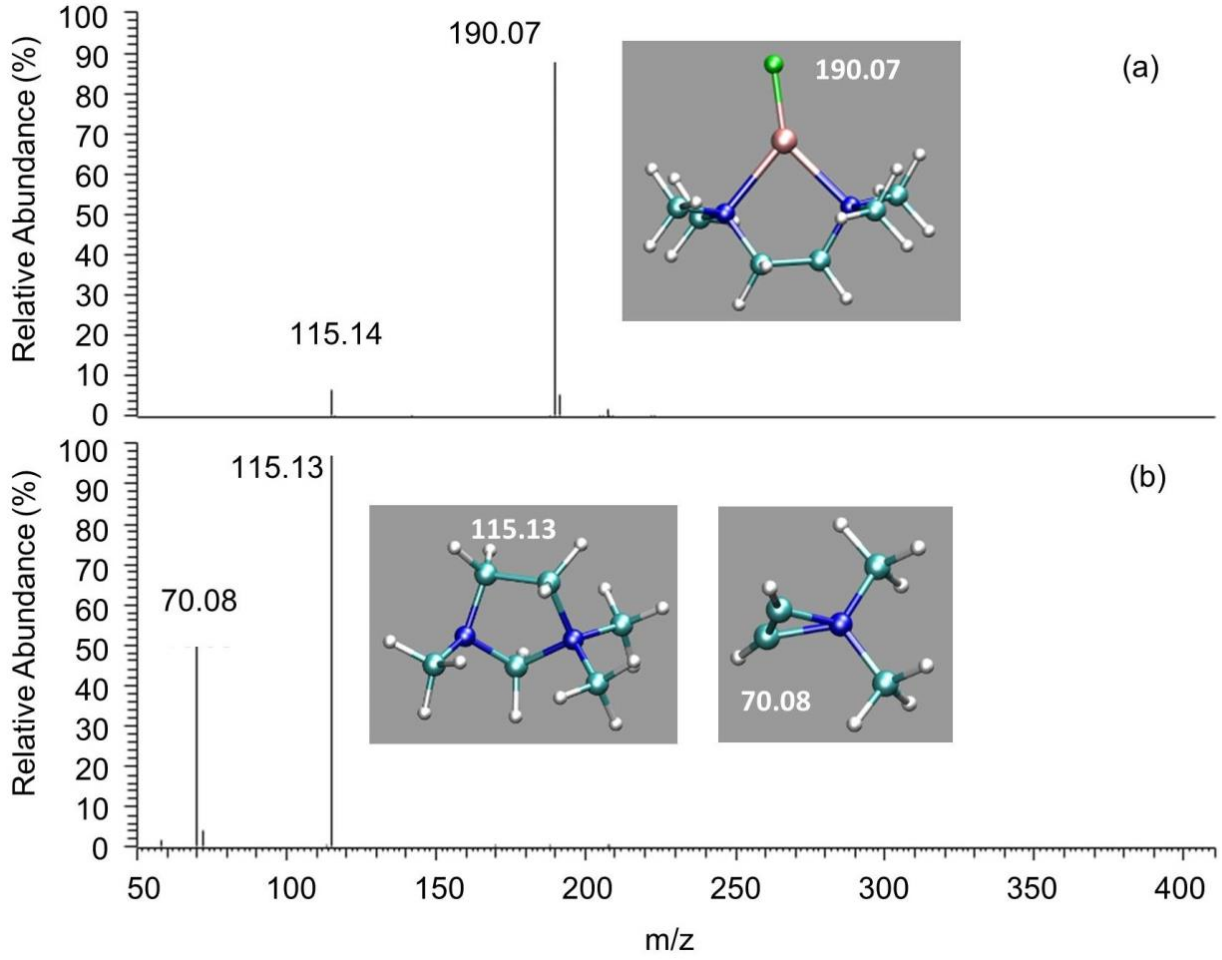


**Figure S5.** (a) $MS^2$ mass spectrum of the $[Mn(hfa)•TMEDA]^+$ ion at *m*/*z* 378, detected in the positive ion mode ESI-MS analysis of $Mn(hfa)_2$•TMEDA methanolic solutions. (b) $MS^3$ mass spectrum of the ion at *m*/*z* 190.07. The structures for the ionic species at *m*/*z* = 190.07, 115.13 and 70.08, obtained from geometry optimization, are also reported. The Mn-containing fragment (*m*/*z* = 190.07) was found to be in the sextet spin state (energy stabilization of the sextet with respect to quartet and doublet: 36.8 kcal×mol$^{-1}$ and 142.2 kcal×mol$^{-1}$, respectively). Atom color codes as in Figure S1.

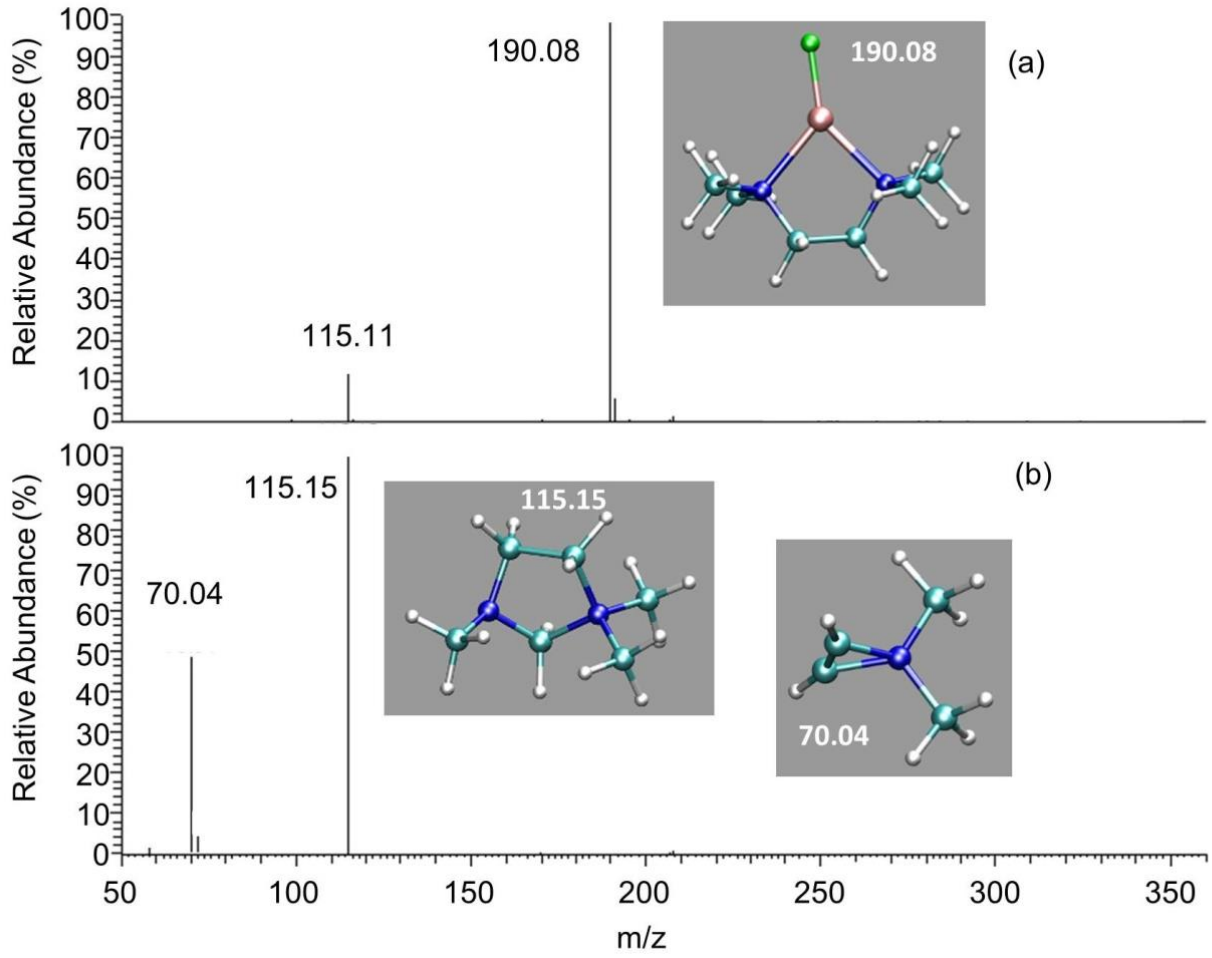


**Figure S6.** (a) $MS^2$ mass spectrum of the $[Mn(tfa)•TMEDA]^+$ ion at *m*/*z* 324, detected in the positive ion mode ESI-MS analysis of $Mn(tfa)_2$•TMEDA methanolic solutions. (b) $MS^3$ mass spectrum of the ion at *m*/*z* 190.08. The structures for the ionic species at *m*/*z* = 190.08, 115.15 and 70.04, obtained from geometry optimization, are also reported. The Mn-containing fragment (*m*/*z* = 190.08) was found to be in the sextet spin state. Atom color codes as in Figure S1.

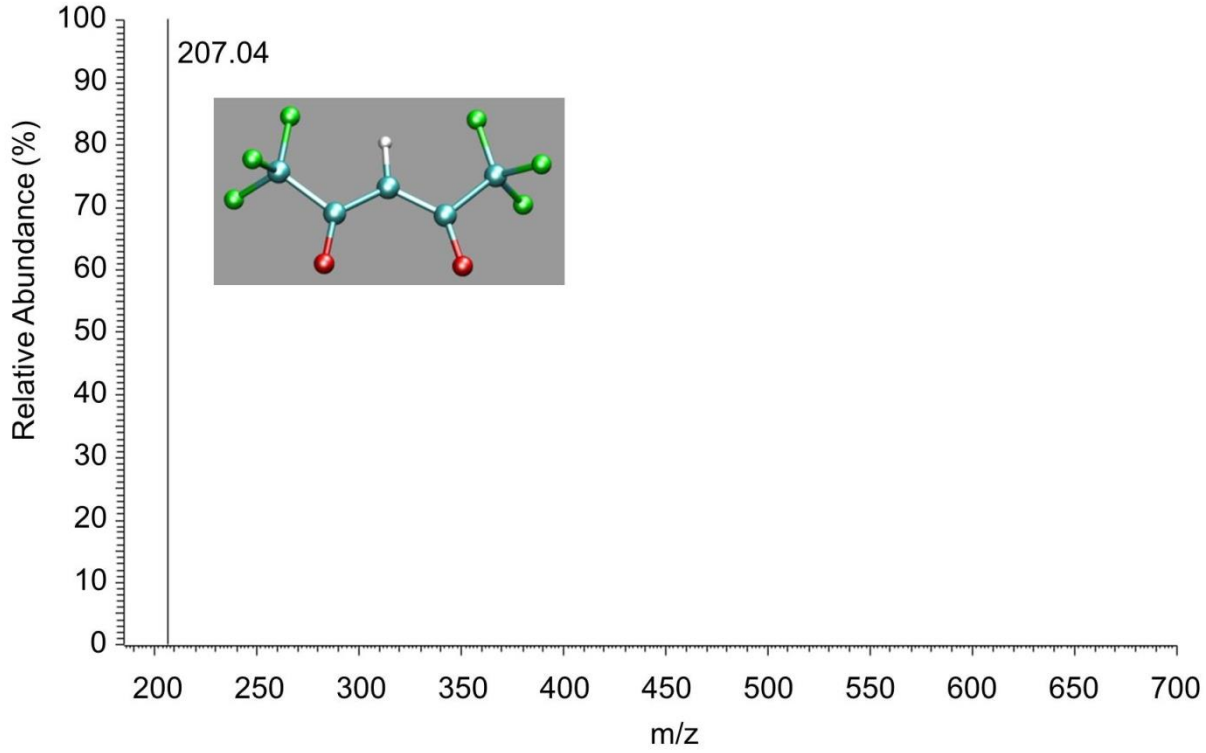


**Figure S7.** $MS^2$ mass spectrum of the $[Mn(hfa)_3]^-$ ion at *m*/*z* 676, detected in the negative ion mode ESI-MS analysis of $Mn(hfa)_2$•TMEDA methanolic solutions. The structure for the ionic species at *m*/*z* = 207.04 obtained from geometry optimization is also reported. Atom color codes as in Figure S1.

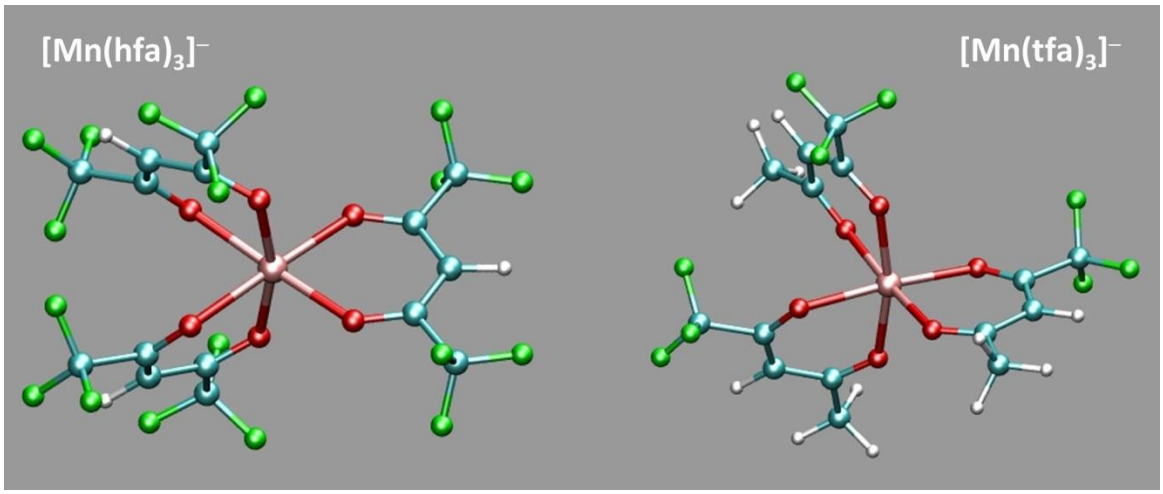


**Figure S8.** Graphical representation of the calculated optimized structure of $[Mn(hfa)_3]^-$ and $[Mn(tfa)_3]^-$ ions. Both structures are stable minima with no imaginary frequency, and the spin state is a sextet. Atom color codes as in Figure S1.

**Comment to Figure S8.** The formation energy $\Delta E_f$ of the $[Mn(L)_3]^-$ anions (L=hfa/tfa) was calculated according to the equation $Mn(L)_2 + L^- \rightarrow [Mn(L)_3]^-$ with the same computational setup described in the Simulation section, by keeping into account the zero point energy contribution and using counterpoise corrections for the basis set superposition errors. The calculated values $\Delta E_f$ amounted to –25.2 and –23.2 kcal×mol$^{-1}$ for $[Mn(hfa)_3]^-$ and $[Mn(tfa)_3]^-$, respectively, by adopting a polarizable continuum model for the solvent (methanol).[2] The values of the formation energies calculated in vacuum were –52.3 and –44.9 kcal×mol$^{-1}$for $[Mn(hfa)_3]^-$ and $[Mn(tfa)_3]^-$, respectively. Hence, both in vacuum and in methanol, the energy gain for the formation of the $[Mn(L)_3]^-$ adduct resulted to be higher in the case of $[Mn(hfa)_3]^-$.

## 4. XPS analysis

XPS characterization was performed using a Perkin–Elmer Φ 5600ci apparatus, with a non-monochromatized AlKα source (hν = 1486.6 eV). Binding energy (BE) values were corrected for charging phenomena by assigning a position of 284.8 eV to the C1s photopeak of adventitious carbon.[3] Atomic percentages were evaluated using sensitivity factors provided by Φ V5.4A.

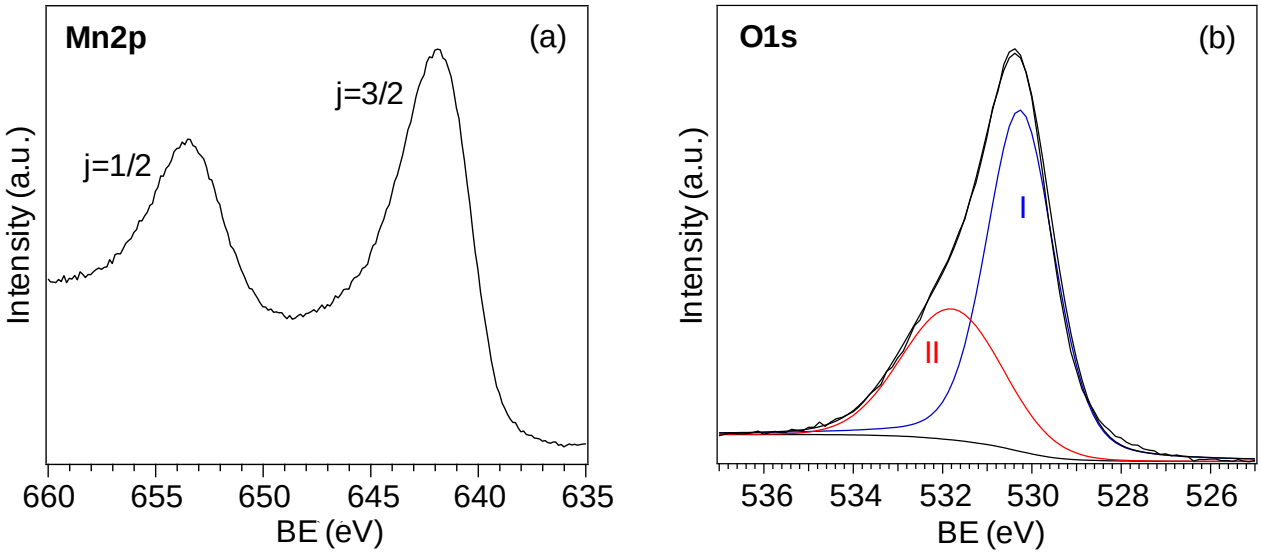


**Figure S9.** Surface Mn2p (a) and O1s (b) photopeaks for a representative $Mn_3O_4$ nanodeposit obtained at 400°C on Si(100), from $Mn(hfa)_2$•TMEDA.

Regardless of the adopted growth temperature, substrate and precursor nature, all the spectra were dominated by the presence of manganese and oxygen signals. Figure S9 displays the Mn2p and O1s surface peaks for a representative specimen. The Mn2p signal [BE($Mn2p_{3/2}$) = 641.9 eV] and spin-orbit splitting separation [Δ(BE) = 11.5 eV][4] were consistent with the presence of $Mn_3O_4$ free from other Mn-containing oxides, as also confirmed by the Mn3s multiplet splitting value (5.4 eV).[5] Accordingly, the principal O1s contribution (I; BE = 530.2 eV) was attributed to lattice oxygen in $Mn_3O_4$, whereas a second band (II) located at BE = 531.8 eV could be ascribed to adsorbed –OH groups and/or carbonate species due to air exposure.[5a,b]

## 5. References

[1] a) L. Goodman, R. R. Sauers, *J. Comput. Chem.* **2007**, *28*, 269-275; b) A. E. Reed, L. A. Curtiss, F. Weinhold, *Chem. Rev.* **1988**, *88*, 899-926; c) E. D. Glendening, J. K. Badenhoop, A. E. Reed, J. E. Carpenter, J. A. Bohmann, C. M. Morales, F. Weinhold, in *NBO 5.0, Theoretical Chemistry Institute, University of Wisconsin, Madison, USA*, **2001**.

[2] M. Cossi, V. Barone, B. Mennucci, J. Tomasi, *Chem. Phys. Lett.* **1998**, *286*, 253-260.

[3] D. Briggs, M. P. Seah, in *Practical surface analysis: Auger and X-ray photoelectron spectroscopy*, John Wiley & Sons: New York, 2nd ed., **1990**.

[4] C. Anil, G. Madras, *J. Mol. Catal. A: Chem.* **2016**, *424*, 106-114.

[5] a) J. F. Moulder, W. F. Stickle, P. E. Sobol, K. D. Bomben, in *Handbook of X-ray photoelectron spectroscopy*, Perkin Elmer Corperation, Eden Prairie, MN, USA, **1992**; b) http://srdata.nist.gov/xps; c) M. Chigane, M. Ishikawa, *J. Electrochem. Soc.* **2000**, *147*, 2246-2251.